Phase-subtraction cell-counting method for live mouse embryos beyond the eight-cell stage

William C. Warger II
Northeastern University
Department of Electrical and Computer Engineering
440 Dana Building
360 Huntington Avenue
Boston, Massachusetts 02115
    and
The Bernard M. Gordon Center for Subsurface Sensing
    and Imaging Systems
Stearns Center, Suite 302
360 Huntington Avenue
Boston, Massachuesetts 02115
E-mail: wwarger@ece.neu.edu

Judith A. Newmark
Carol M. Warner
Northeastern University
Department of Biology
134 Mugar Building
360 Huntington Avenue
Boston, Massachusetts 02115
    and
The Bernard M. Gordon Center for Subsurface Sensing
    and Imaging Systems
Stearns Center, Suite 302
360 Huntington Avenue
Boston, Massachuesetts 02115

Charles A. DiMarzio
Department of Electrical and Computer Engineering
440 Dana Building
360 Huntington Avenue
Boston, Massachusetts 02115
    and
The Bernard M. Gordon Center for Subsurface Sensing
    and Imaging Systems
Stearns Center, Suite 302
360 Huntington Avenue
Boston, Massachuesetts 02115

Abstract. Since 1978 *in vitro* fertilization (IVF) procedures have resulted in the birth of over 3 million babies. Yet in 2005, IVF procedures had a live birth rate of only 34%, with 32% of these births resulting in multiple pregnancies. These multiple pregnancies were directly attributed to the transfer of multiple embryos to increase the probability that a single, healthy embryo was included. The predominantly accepted noninvasive viability markers for embryos created by IVF are (1) number of cells at specific time points during development and (2) overall morphology of the embryo. Currently, it is difficult to count the number of cells beyond the eight-cell stage noninvasively. We report a nontoxic cell-counting method capable of counting cell numbers ranging from 8 to 26 in live mouse embryos. This method is derived from the fusion of differential interference contrast and optical quadrature microscopy and is verified by epifluorescence images of Hoechst-stained nuclei. The phase-subtraction cell-counting method is the first accurate, nontoxic technique to count cells through the morula stage in mouse embryos and may enhance the use of cell number as a viability marker if adopted for use with human embryos in the IVF clinic. © *2008 Society of Photo-Optical Instrumentation Engineers.* [DOI: 10.1117/1.2937468]

Keywords: phase-subtraction cell-counting method; optical quadrature microscopy; quadrature tomographic microscopy; differential interference contrast; embryo viability; *in vitro* fertilization.

1 Introduction

In the United States, one in six couples suffers from problems related to infertility.[1] Assisted reproductive technologies (ART), such as *in vitro* fertilization (IVF), have given these couples a second option after natural attempts at reproduction have proven unsuccessful. However, after more than a quarter century of administered IVF procedures that have resulted in over three million babies, U.S. clinics were still only able to provide a live birth rate of 34% with fresh nondonor eggs or embryos in 2005.[2] A major cause of the low success rate is the inability to determine which embryos are viable and will lead to a successful pregnancy. As a result, clinicians transfer multiple embryos to increase the chances of including one viable

embryo that will produce a successful pregnancy. In 2005, 32% of successful IVF procedures also resulted in multiple pregnancies because three or more embryos were transferred in 47% of procedures and four or more embryos were transferred[2] in 18%. This practice introduces complications for both mother and child. Multiple pregnancy leads to the increased risk of pregnancy complications, including preterm delivery, prematurity, low birth weight, congenital malformations, and infant death.[2–10] Multiple-birth infants from IVF also face an increased risk of neurological problems, especially cerebral palsy.[2,11] For all of these reasons, there is a worldwide effort toward single embryo transfer.[12,13]

Human embryos that are cultured in IVF clinics are given a grade based on two major criteria: (1) the number of cells at specific time points during development and (2) overall morphology.[14–26] Some of the morphological parameters that

---

Address all correspondence to William Warger II, Electrical and Computer Engineering, Northeastern University, 440 Dana Building - 360 Huntington Ave, Boston, MA 02115 United States of America; Tel: 6173738570; Fax: 6173737783; E-mail: wwarger@ece.neu.edu

have been considered are symmetry, size, fragmentation, vacuoles, perivitelline space, position of pronuclei, orientation of nucleoli, thickness and structure of the zona pellucida, and spindle integrity, but none of these parameters has proven to be good enough to determine embryo viability reliably. There is agreement that the first criterion, embryo cell number, shows that faster developing embryos are more likely to give rise to a successful pregnancy than slower developing embryos.[22–24] However, current nontoxic microscopy techniques are unable to count the number of cells accurately past the eight-cell stage. Thus, the number of cells can be used for day 3 transfers where embryos containing less than 10 cells are returned to the uterine environment, but cannot be used for blastocyst stage transfers that occur on day 5 of development. Blastocyst transfers are advantageous because the embryo does not reach the uterus until day 5 in a natural pregnancy,[27] and the ability to develop to the blastocyst stage is also a viability marker.[28] As a result, the decision on embryo quality in blastocyst transfers is based on morphological markers such as the expansion of the blastocoel cavity and the characteristics of the inner cell mass and the trophectoderm.[28] Therefore, the creation of hardware and software that could noninvasively count the number of cells after the eight-cell stage may enable the number of cells to be included among the criteria for blastocyst stage transfers.

The Keck three-dimensional fusion microscope (3DFM) at Northeastern University combines differential interference contrast, epifluorescence, optical quadrature, laser scanning confocal fluorescence and reflectance, and two-photon fluorescence microscopy on a Nikon TE2000U base.[29] The nontoxic cell-counting method presented in this paper utilizes the fusion of optical quadrature microscopy (OQM) and differential interference contrast (DIC) microscopy to acquire and process the images necessary to count the number of cells in mouse embryos beyond the eight-cell stage of development. The details of the hardware and software used to accomplish this goal are presented in this paper.

2 Imaging Modalities

2.1 DIC

DIC microscopy produces images in which contrast is related to a component of the gradient of optical path length along a specified direction.[30] Clinicians currently use DIC, or the similar Hoffman optics,[30] to analyze the morphological characteristics of embryos and to make their best determination of the number of cells in the embryo noninvasively. A DIC image of an embryo provides distinct cell boundaries for cells within the depth of field because the cell boundaries provide the greatest difference in optical path between the two waves. However, as the embryo develops, the cells begin to overlap and the edges from the bottom layer of cells are obstructed by the top layer. Cell edges are visible under a single layer of overlapped cells, providing the ability to count accurately up to two layers of four cells in an eight-cell embryo. Once the embryo begins to form a third layer, the cell edges of the bottom layer cannot be resolved, thereby making accurate cell counts unattainable by using DIC microscopy alone. Additional techniques have been developed to reconstruct quantitative phase information from DIC images, but they have not been applied to large biological samples greater than 20 μm
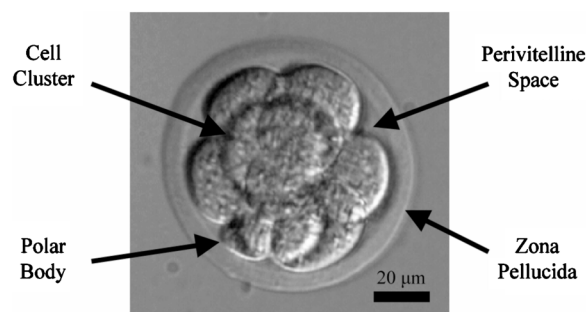
Fig. 1 DIC image of a live mouse embryo. The zona pellucida surrounds the developing cells and polar body.

in diameter.[31–36] The diameter of a mouse embryo is approximately 100 μm, including the zona pellucida, and the diameter of a human embryo is[22] approximately 130 μm.

A DIC image of a typical eight-cell live mouse embryo is shown in Fig. 1. Mice are an excellent animal model for human research and have been classified as a model organism by the National Institutes of Health. The mouse model provides many advantages over human embryos for research, including genetically identical inbred mouse strains, embryo availability, and low cost.[37] Early mouse embryo development is very similar to human embryo development. Each cell, or blastomere, cleaves into two cells with a combined volume approximately equal to the original cell before division. Therefore, the total volume of the embryo is relatively constant during preimplantation development. The first polar body extrudes during meiosis and degenerates shortly after fertilization of the oocyte. The second polar body extrudes on fertilization and is maintained at least through the eight-cell stage of development, after which it begins to degenerate. The second polar body can be easily distinguished from the blastomeres because it is considerably smaller in size compared to the developing cells. The zona pellucida is a spherical encasement with a thickness of approximately 7 μm that surrounds the cells and polar body and keeps them contained. The space between the blastomeres and the zona pellucida is the perivitelline space. During imaging, we have assumed that the perivitelline space is filled with culture medium since the zona pellucida is a loose matrix that is porous to macromolecules, including proteins.

2.2 Fluorescence Microscopy

Fluorescence microscopy images the distribution of individual molecules by collecting only the fluorescent wavelengths that are emitted after excitation with a particular band of wavelengths.[30] Hoechst 33342 dye [Intergen (Millipore), Billerica, Massachusetts] was used to bind fluorophores to the nucleus of each cell to image the distribution of nuclei within the embryo. A piezoelectric z stage (Piezosystems Jena, Jena, Germany) was used to step the embryo through the focus of the objective to provide a z stack of images through the sample. Counting the stained nuclei within the z stack provides the ground truth for the number of nuclei within an embryo and was used to determine the total number of cells.[38] This method of cell counting is easy to use and offers a relatively fast measurement for the number of cells, but the Ho-

echst stain permanently binds to the DNA of the nuclei and is a known mutagen. Its use is therefore considered an invasive and potentially mutagenic procedure that is not permitted in a clinical setting. We have used this method only to determine the number of cells in each embryo to analyze the success of our cell-counting procedure. It is important to note that two-photon or confocal fluorescence microscopy can also be used to image the Hoechst stained nuclei, but the epifluorescence images provided sufficient image quality to obtain accurate cell counts.

2.3 OQM

OQM noninvasively reconstructs the amplitude and phase of an optically transparent sample.[39–42] An OQM image of a sample that creates a change in phase greater than 2π, such as a mouse embryo, must be unwrapped using a 2-D phase-unwrapping algorithm to produce a quantitative image. The OQM images of mouse embryos were unwrapped using the algorithm L^p-norm.[43] The image of unwrapped phase was then multiplied by $\lambda/2\pi$, where λ is equal to 633 nm, to provide an image of optical path difference (OPD image). Using a projection model that neglects diffraction, the total optical path length (OPL) within the image is related to the sum of the indices of refraction (n) along the path by

$$\text{OPL} = \sum_{m=1}^{N} \int_{0}^{h_m(x,y)} [n_m(x,y,z) - n_0]\, dz \qquad (1)$$

where $h_m(x,y)$ is the local physical thickness of the sample in the z direction having index of refraction n_m, n_0 is the index of refraction of the medium that defines zero OPL, and N is the number of different indices of refraction in the path. However, the absolute phase of the reference is unknown so the images are interpreted as a relative mapping of OPL. Ambiguities also exist between n and z because an object with a certain thickness and index of refraction will appear the same as an object with half of the thickness and twice the index. As a result, we interpret the images as the OPDs between the various biological elements, where the overall OPD corresponds to the difference between the optical path through the object and through an equal thickness of culture medium.

Note that other quantitative phase imaging techniques, such as polarization interferometers,[44] digital holography,[45–47] Fourier phase microscopy,[48] Hilbert phase microscopy,[49] phase-shifting interferometry[50,51] (PSI), quantitative phase microscopy[52–54] (QPM), and additional polarization-based techniques[55,56] could replace OQM and provide the quantitative phase information for this cell-counting method, assuming these systems produce comparable image quality with mouse embryos that are 100 μm in diameter.

3 Phase-Subtraction Cell-Counting Method

The phase-subtraction cell-counting method utilizes the combination of two nontoxic imaging modalities, OQM and DIC, to image and count the number of cells within live mouse embryos.[42] The OQM image provides the thickness of the sample in the z direction by Eq. (1), and the DIC image provides distinct cell boundaries in the xy image plane.

The OQM image was converted into an image of OPD and observed side-by-side with the DIC image, as shown in Fig. 2,
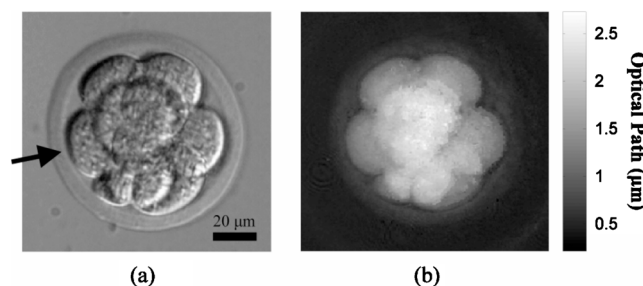
Fig. 2 (a) DIC and (b) OPD images of a live mouse embryo. The arrowed cell was chosen as the reference cell because it has the least amount of cell overlap in the DIC image and a uniform distribution of optical path in the OPD image.

to choose a reference cell that would provide the total OPD of a single cell. The total OPD of the cell is related to the diameter of the ellipsoidal cell in the z direction. Ideally, the reference cell was along the perimeter of the embryo, not overlapped by other cells, and the same size as the other visible cells. In Fig. 2(a), the cell to the left, marked by an arrow, was chosen because approximately half of the cell appeared to have no overlap with other cells in the DIC image and it had a uniform distribution of optical path in the OPD image. Nonuniformities within the OPD image could correspond to cell overlap or fragmentation not visible in the DIC image, which may introduce errors when calculating the total OPD for a single cell.

A line was drawn on the DIC image in Fig. 3(a) that traversed from the culture medium, through the zona pellucida and the center of the reference cell, to an overlapped region of cells. Ideally a cell with no overlap would have been chosen, but that was not possible in embryos beyond the eight-cell stage because every cell was overlapped by another cell. Therefore, the line continued through the nonoverlapped region of the cell and into the cell overlap to produce the most accurate fit. The optical path along the line drawn on the DIC image in Fig. 3(a) was plotted in Fig. 3(b) and labeled according to the biological origins. At the bottom of the plot is a flat line of constant amplitude that was within the noise level of the image and represented the contribution of optical path from the culture medium. As the line on the DIC image started to cross the zona pellucida, the plot began to increase
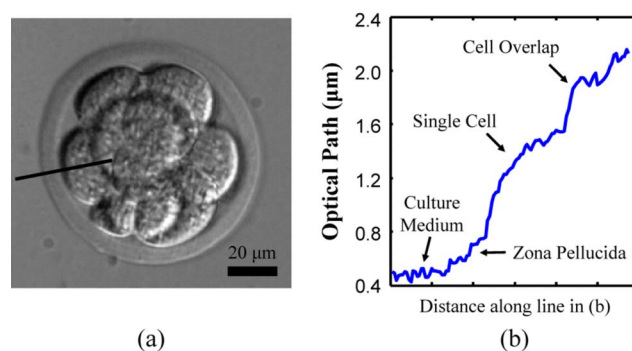
Fig. 3 (a) Line drawn on the DIC image to plot the optical path through the center of the reference cell in (b). The plot is labeled to relate the optical path to the biological origins.

(a)   (b)
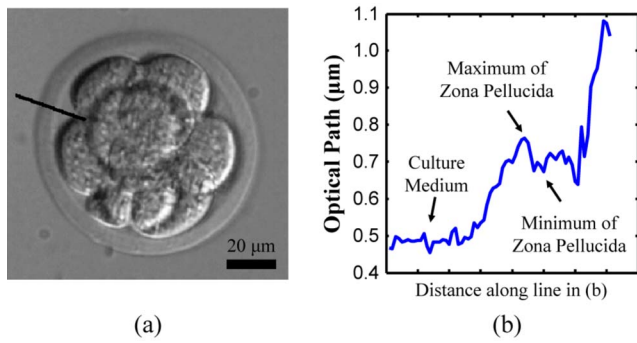
Fig. 4 (a) Line drawn on the DIC image to plot the optical path for the zona pellucida and perivitelline space in (b). The minimum optical path of the reference cell is equal to the minimum optical path of the zona pellucida.

following a quasiparabolic shape toward a maximum point where the line reached the inside border of the zona pellucida. The optical path increased again in a parabolic fashion once the line reached the cell, and continued until the line reached the region of overlapped cells. A full parabola would have been seen if the reference cell had not been overlapped by another cell.

A point was selected manually on the plot in Fig. 3(b) that represented the minimum optical path of the reference cell. Since the zona pellucida is an encasement that surrounds the developing cells, there was some contribution from the top and bottom halves that was less than the optical path of the inside edge of the zona pellucida that touched the cell, but more than the optical path of the culture medium. Figure 4(a) shows a line drawn on the DIC image that crosses the zona pellucida and a portion of the perivitelline space, and ends within the developing cells. The plot in Fig. 4(b) shows that the optical path along the line increases as the line crosses the zona pellucida and then reaches a local maximum point when the line reaches the inside edge of the zona pellucida. As the line continues, the plot of the optical path reaches a local minimum and then increases again when the line reaches the developing cells. The local minimum was defined as the minimum optical path of the reference cell because there were no cells in this region of the DIC image and the perivitelline space was assumed to be filled with culture medium. The minimum optical path of the reference cell was approximated as 3/4 of the optical path between the culture medium and the observed maximum value associated with the zona pellucida in the plot shown previously in Fig. 3(b) to alleviate the necessity to produce two separate plots.

Five additional points were selected manually along the parabolic shape in Fig. 3(b) to achieve a parabolic fit that represented the optical path of the reference cell. The maximum optical path of the reference cell was recorded as the maximum point along the parabola created by the fit. The total OPD of a single cell was defined as the difference between the calculated maximum and the approximated minimum values of optical path for the reference cell.

The OPD and DIC images were once again observed side-by-side to determine the elliptical boundary of the cell. Three points were selected for the center of the ellipse, the minimum radius of the ellipse (a), and the maximum radius of the el-

(a)   (b)
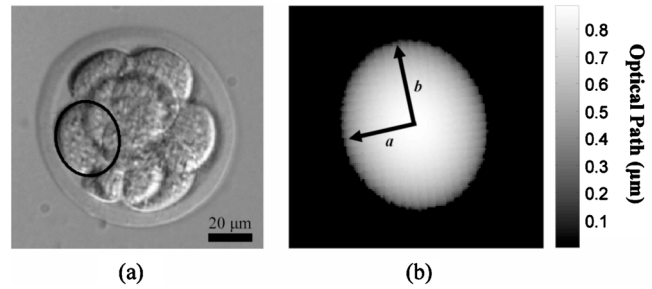
Fig. 5 (a) Cell boundary created for the reference cell and (b) ellipsoidal model cell of optical path created from the combination of the cell boundary and the total OPD of a single cell.

lipse (b). An ellipse was created from these three points and displayed on the DIC image to confirm a proper fit, as shown in Fig. 5(a). Combining the radii of the ellipse with the total OPD of a single cell (c) created an ellipsoidal model cell of optical path in Fig. 5(b). The total OPD of a single cell was used to subtract only positive optical path from the OPD image.

The equation for a perfect ellipsoid,

$$\frac{x^2}{a^2} + \frac{y^2}{b^2} + \frac{z^2}{c^2} = 1,\qquad(2)$$

and the equation for a slightly flattened ellipsoid,

$$\left(\frac{x^2}{a^2} + \frac{y^2}{b^2}\right)^2 + \frac{z}{c} = 1,\qquad(3)$$

were the two equations analyzed empirically that produced the best fit for cells in the OPD image. In these equations, z is the optical path parallel to the optical axis of the microscope, a and b are the radii chosen for the elliptical cell boundary, c is the total OPD for a single cell, and x and y are projections of the basis axes related to the chosen directions of a and b in the 2-D image plane. The method assumed all cells had the same total OPD in the z direction so all model cells used the same value for c. A plot of the cross section of optical path for a theoretical cell created by Eqs. (2) and (3) with $y=0$, $a=1$, and $c=1$ is shown in Fig. 6(a). The dashed line (--) is the optical path for Eq. (2) and the solid line is the optical path for Eq. (3). A plot of the cross section of the same cell with Eqs.

(a)   (b)
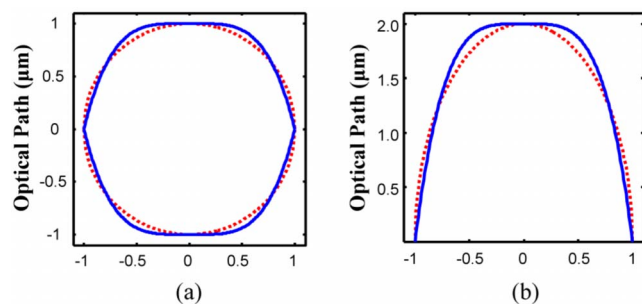
Fig. 6 (a) Plot of the cross section of optical path for model cells created by Eq. (2) with a dashed line (--) and Eq. (3) with a solid line and (b) plot of the cross section of positive optical path for the model cells that are subtracted from the OPD image.
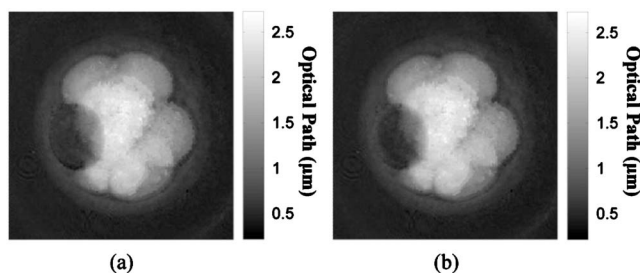
Fig. 7 (a) Subtraction of the model cell created with (a) a perfect ellipsoid [Eq. (2)] and (b) a flattened ellipsoid [Eq. (3)] from the OPD image.

Fig. 8 Final subtracted OPD image with the minimum colorbar value set to the minimum optical path of the reference cell. A polar body remains in the bottom left quadrant, which is significantly smaller than the size of the previous cells selected in the DIC image.

(2) and (3) in terms of z and $c=2$ is presented in Fig. 6(b) to show the positive OPD that would be subtracted for the theoretical cell. Figure 7(a) shows that the subtraction of a model cell created by Eq. (2) produced a visible discontinuity at the boundary of the reference cell, whereas Fig. 7(b) shows the subtraction of a model cell created by Eq. (3) produces a softer edge at the boundary. Equation (3) for a flattened ellipsoid was chosen for the model cells primarily because many cells were pressed against each other and against the zona pellucida, and as such, could not be fit with perfect ellipsoidal boundaries. This can be seen in Fig. 1, where all but two visible cells have irregularly shaped boundaries. Equation (3) was also chosen because the depth of field of the DIC image may have caused errors in the location of the created cell boundaries. A larger depth of field provides more visible boundaries within the image, but the out-of-focus boundaries are more likely to be blurred, leading to potential errors in the exact locations of the created boundaries. A smaller depth of field provides fewer visible boundaries, but the created boundaries will be more accurate in location. Thus, the softer subtraction at the boundary created by Eq. (3) was considered more appropriate to alleviate potential errors when the cell boundaries were created on the DIC image. There is still much to be learned about the shape of the cells, especially in the z direction, and the effect of cell shape on the optical path will be the subject of future experimentation.

When the model cell was subtracted from the OPD image, either the background culture medium and zona pellucida or additional optical path associated with cells overlapped with the subtracted cell was revealed. Elliptical boundaries were created for all cells visible in the DIC image and subtracted from the OPD image. Once all the visible cells were accounted for, the subtracted OPD image was analyzed for hidden cells that could not be seen in the DIC image. Elliptical boundaries were fit to elliptically shaped regions or clusters with the approximate size of the cells previously subtracted in the OPD image. The approximate size included the combination of the cross-sectional area created by the previous cell boundaries and the total OPD of a single cell. Elliptical boundaries were fit to these clusters and model cells were subtracted until no such clusters remained and the count was complete, as shown in Fig. 8. A complete visualization of the phase-subtraction cell-counting method is provided at http://www.keck3dfm.neu.edu/samplevideo.

A small cluster of optical path still existed in the lower left quadrant of Fig. 8 that corresponded to the polar body previ-

ously labeled in Fig. 1. This cluster was considered a polar body and not a cell because the boundary of the cluster was much smaller than the boundaries of the cells created within the DIC image. Observations of OQM images of live mouse embryos have shown variations of optical path associated with the polar bodies, which may be caused by various levels of degeneration, thereby requiring more study to define additional characteristics to differentiate the polar body from cells in the subtracted OPD image.
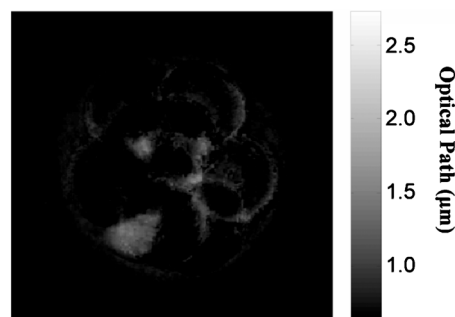
4 Image Collection and Counting Results

We superovulated C57BL/6 female mice (Jackson Laboratory, Bar Harbor, Maine) with equine chorionic gonadotropin (eCG) and human chorionic gonadotropin (hCG) (Sigma, St. Louis, Missouri) to increase the number of eggs,[57] and mated with single CBA/Ca male mice. Plug-positive female mice were sacrificed on days 3 and 4, after hCG injection, and eight-cell through morula stage embryos were collected in M2 medium (Specialty Media, Phillipsburg, New Jersey). The embryos were stained for 30 min in 1 μg/ml Hoechst 33342 dye, which binds to the DNA within the nucleus of each cell. Morphologically normal appearing embryos (no visible fragmentation, intact/healthy appearing zona pellucida and cells) were placed in M2 microdrops, under equilibrated oil, in a Mat-Tek imaging dish with a coverslip-bottom (Mat-Tek, Ashland, Massachusetts). Single images were acquired at the center focus plane of the embryo in DIC and OQM with a 20×, 0.45 numerical aperture (NA) objective lens and a 0.52 NA condenser lens. Center focus was found when the outer boundary of the zona pellucida was in focus. A z stack of images was also acquired of the Hoechst-stained nuclei with epifluorescence, and analyzed using the count cells tool in Metamorph software (Molecular Devices, Downingtown, Pennsylvania) to determine the number of cells. Since the images were not acquired simultaneously and the embryos were live, in culture medium, and moved along the z axis by the piezoelectric z stage for the z stack of epifluorescence images, the OPD and DIC images required registration. Landmarks were chosen visually at the intersection of cells along the perimeter of the embryos because they were easy to locate. Landmarks were not chosen within the embryos because intersections in the OPD image may be created or distorted by cells not visible in the DIC image. An affine transform was

Table 1 Results of cell counts produced by epifluorescence imaging of Hoechst-stained nuclei and the phase-subtraction cell-counting method for a training set of five live mouse embryos where the number of cells was known before the phase-subtraction count was completed.

	Fluorescence Count	Phase-Subtraction Count
1	13 cells	13 cells
2	14 cells	14 cells
3	16 cells	16 cells
4	17 cells	17 cells
5	25 cells	25 cells

calculated from the selected landmarks and applied to one of the images to provide pixel-to-pixel registration.

Phase-subtraction cell counts were completed on 15 morphologically normal, live mouse embryos. The first five samples were used as a training set where the number of cells was known before the cell count was complete. This training set was used to determine the potential variation in cell sizes for embryos with different cell numbers because the cells divide asynchronously.[58] As seen in Table 1, accurate cell counts were obtained for the five samples once the correct cell boundaries were chosen.

The second set of 10 samples was completed blind, where the number of cells remained unknown until after the cell-count was complete. The phase-subtraction cell-counting method had a maximum error of one cell for the 10 blind samples (samples 7 and 8) and accurately counted up to 26 cells, as shown in Table 2. To further analyze the ellipsoid

Table 2 Results of cell counts produced by epifluorescence imaging of Hoechst-stained nuclei and the phase-subtraction cell counting method for 10 live mouse embryos, where the number of cells was not known before the phase-subtraction count was completed.

	Fluorescence Count	Phase-Subtraction Count
1	8 cells	8 cells
2	8 cells	8 cells
3	8 cells	8 cells
4	12 cells	12 cells
5	12 cells	12 cells
6	15 cells	15 cells
7	16 cells	15 cells
8	16 cells	15 cells
9	21 cells	21 cells
10	26 cells	26 cells

Eqs. (2) and (3), the cell counts were repeated with the use of the perfect ellipsoid in Eq. (2), and the same results as presented in Tables 1 and 2 were obtained.

5 Discussion

The phase-subtraction cell-counting method described in this paper is, to our knowledge, the first to produce accurate, non-toxic cell counts in live mouse embryos beyond the eight-cell stage. If applied to human embryos, this method could provide[59] an additional viability marker for embryos during the morula stage on day 4. However, the method is currently time consuming and subjective with respect to how the user perceives and creates the cell boundaries. Overlapped layers of cells may obstruct portions of cell boundaries for cells underneath the top layer. This can be seen in the cell boundary selected in Fig. 5(a). The left boundary of the cell is clearly visible, but the circular cell in the center of the embryo blurs the right boundary. The blurring does not hinder the creation of this particular cell boundary because other cells do not overlap most of the cell, but embryos with a greater number of cells will have larger portions of the cell boundaries obstructed by cell overlap. We are working on image-processing techniques to enhance and automatically determine the cell boundaries in both the DIC and subtracted OPD images to speed up the process and remove the subjective decisions associated with the location of cell boundaries.

We are also refining the phase-subtraction cell-counting method to allow for different thicknesses that are dependent on the size of the individual cells. The assumption that each cell has the same total OPD in the z direction worked for the samples reported in this paper because the final goal was the total number of cells and not an analysis of remnant optical path in the final subtracted image. Embryonic cells do not divide synchronously,[58] so the method must be modified to correct for varying cell sizes between cleavage stages. A higher order ellipsoidal model cell that fits arbitrarily flattened boundaries could perfect the subtraction and potentially provide a meaningful analysis of the remnant optical path in the final subtracted image. This analysis could provide information on parameters such as degree of fragmentation and the location of the polar body. However, additional work must be completed to provide a better understanding of imaging mouse embryos with OQM. The assumption that there are no diffraction effects in Eq. (1) does not hold for samples with large changes in index compared to the immersion medium or when imaging thick samples. Thus, refraction and depth-of-field effects must be analyzed to perfect and increase the versatility of the method.

An important potential advantage of the phase-subtraction cell-counting method is that the phase imaging instrumentation was incorporated within a general microscope used for DIC imaging. Thus, the creation of a bolt-on instrument for various commercial microscopes would enable the clinician to analyze the other viability markers in the usual manner and include the cell-counting procedure by acquiring one additional image of quantitative phase while the embryo is on the same stage. Several other instruments provide the analysis of additional viability markers, but they require the purchase of a separate instrument.

In conclusion, the nontoxic phase-subtraction cell-counting method has produced accurate cell counts in live mouse embryos with cell numbers ranging from 8 to 26. Additional work must be completed to improve the ease of use and processing time, but if verified and applied to human embryos, this method could provide an additional viability marker that may increase the clinician's ability to determine embryo viability for IVF procedures.

References

1. A. Chandra, G. M. Martinez, W. D. Mosher, J. C. Abma, and J. Jones, "Fertility, family planning, and reproductive health of U.S. women: data from the 2002 National Survey of Family Growth," *Vital Health Stat. 23* Series **23** No. (24), 2–23 (2005).
2. Centers for Disease Control and Prevention, American Society for Reproductive Medicine, Society for Assisted Reproductive Technology, *2005 Assisted Reproductive Technology Success Rates: National Summary and Fertility Clinic Reports*, Centers for Disease Control and Prevention, Atlanta GA (2007).
3. J. A. Martin and M. M. Park, "Trends in twin and triplet births: 1980-1997," *Natl. Vital Stat. Rep.* **47**(24), 1–16 (1999).
4. ESHRE Campus Course Report, "Prevention of twin pregnancies after IVF/ICSI by single embryo transfer," *Hum. Reprod.* **16**(4), 790–800 (2001).
5. O. Ozturk, S. Bhattacharya, and A. Templeton, "Avoiding multiple pregnancies in art: evaluation and implementation of new strategies," *Hum. Reprod.* **16**(7), 1319–1321 (2001).
6. D. De Neubourg, K. Mangelschots, E. Van Royen, M. Vercruyssen, G. Ryckaert, M. Valkenburg, J. Barudy-Vasquez, and J. Gerris, "Impact of patients' choice for single embryo transfer of a top quality embryo versus double embryo transfer in the first IVF/ICSI cycle," *Hum. Reprod.* **17**(10), 2621–2625 (2002).
7. J. Gerris, D. De Neubourg, K. Mangelschots, E. Van Royen, M. Vercruyssen, J. Barudy-Vasquez, M. Valkenburg, and G. Ryckaert, "Elective single day 3 embryo transfer halves the twinning rate without decrease in the ongoing pregnancy rate of an IVF/ICSI programme," *Hum. Reprod.* **17**(10), 2626–2631 (2002).
8. A. G. Sutcliffe, *IVF Children: The First Generation*, Parthenon Publishing, New York (2002).
9. E. Nowak, I. Blickstein, E. Papiernik, and L. Keith, "Iatrogenic multiple pregnancies: do they complicate perinatal care?" *J. Reprod. Med.* **48**(8), 601–609 (2003).
10. D. M. Kissin, L. A. Schieve, and M. A. Reynolds, "Multiple-birth risk associated with IVF and extended embryo culture: USA, 2001," *Hum. Reprod.* **20**(8), 2215–2223 (2005).
11. B. Strömberg, G. Dahlquist, A. Ericson, O. Finnström, M. Köster, and K. Stjernqvist, "Neurological sequelae in children born after in-vitro fertilisation: a population-based study," *Lancet* **359**(9305), 461–465 (2002).
12. T. Gurgan and A. Demirol, "Why and how should multiple pregnancies be prevented in assisted reproduction treatment programmes?" *Reprod. Biomed. Online* **9**(2), 237–244 (2004).
13. L. A. Schieve, "The promise of single-embryo transfer," *N. Engl. J. Med.* **354**(11), 1190–1193 (2006).
14. J. M. Cummins, T. M. Breen, K. L. Harrison, J. M. Shaw, L. M. Wilson, and J. F. Hennessey, "A formula for scoring human embryo growth rates in in vitro fertilization: its value in predicting pregnancy and a comparison with visual estimates of embryo quality," *J. In Vitro Fert Embryo Transf* **3**(5), 284–295 (1986).
15. F. Puissant, M. Van Rysselberge, P. Barlow, J. Deweze, and F. Leroy, "Embryo scoring as a prognostic tool in IVF treatment," *Hum. Reprod.* **2**(8), 705–708 (1987).
16. V. N. Bolton, S. M. Hawes, C. T. Taylor, and J. H. Parsons, "Development of spare human preimplantation embryos in vitro: an analysis of the correlations among gross morphology, cleavage rates, and development to blastocyst," *J. In Vitro Fert Embryo Transf* **6**(1), 30–35 (1989).
17. S. Ziebe, K. Petersen, S. Lindenberg, A. G. Andersen, A. Gabrielsen, and A. N. Andersen, "Embryo morphology or cleavage stage: how to select the best embryos for transfer after in-vitro fertilization," *Hum. Reprod.* **12**(7), 1545–1549 (1997).
18. D. K. Gardner and W. B. Schoolcraft, "Culture and transfer of human blastocysts," *Curr. Opin. Obstet. Gynecol.* **11**(3), 307–311 (1999).
19. J. Tesarik and E. Greco, "The probability of abnormal preimplantation development can be predicted by a single static observation on pronuclear stage morphology," *Hum. Reprod.* **14**(5), 1318–1323 (1999).
20. C. Racowsky, K. V. Jackson, N. A. Cekleniak, J. H. Fox, M. D. Hornstein, and E. S. Ginsburg, "The number of 8-cell embryos is a key determinant for selecting day 3 or day 5 transfer," *Fertil. Steril.* **73**(3), 558–564 (2000).
21. L. Scott, R. Alvero, M. Leondires, and B. Miller, "The morphology of human pronuclear embryos is positively related to blastocyst development and implantation," *Hum. Reprod.* **15**(11), 2394–2403 (2000).
22. C. M. Warner and C. A. Brenner, "Genetic regulation of preimplantation embryo survival," *Curr. Top Dev. Biol.* **52**, 151–192 (2001).
23. T. Baczkowski, R. Kurzawa, and W. Glabowski, "Methods of embryo scoring in *in vitro* fertilization," *Reprod. Biol.* **4**(1), 5–22 (2004).
24. C. M. Warner, J. A. Newmark, M. Comiskey, S. R. De Fazio, D. M. O'Malley, M. Rajadhyaksha, D. J. Townsend, S. McKnight, B. Roysam, P. J. Dwyer, and C. A. DiMarzio, "Genetics and imaging to assess oocyte and preimplantation embryo health," *Reprod. Fertil. Dev.* **16**(7), 729–741 (2004).
25. Y. Shen, T. Stalf, C. Mehnert, U. Eichenlaub-Ritter, and H. R. Tinneberg, "High magnitude of light retardation by the zona pellucida is associated with conception cycles," *Hum. Reprod.* **20**(6), 1596–1606 (2005).
26. Y. Shen, T. Stalf, C. Mehnert, L. De Santis, I. Cino, H. R. Tinneberg, and U. Eichenlaub-Ritter, "Light retardance by human oocyte spindle is positively related to pronuclear score after ICSI," *Reprod. Biomed. Online* **12**(6), 737–751 (2006).
27. D. K. Gardner and M. Lane, "Culture and selection of viable blastocysts: a feasible proposition for human IVF?" *Hum. Reprod. Update* **3**(4), 367–382 (1997).
28. B. Balaban, K. Yakin, and B. Urman, "Randomized comparison of two different blastocyst grading systems," *Fertil. Steril.* **85**(3), 559–563 (2006).
29. W. C. Warger, II, G. S. Laevsky, D. J. Townsend, M. Rajadhyaksha, and C. A. DiMarzio, "Multimodal optical microscope for detecting viability of mouse embryos *in vitro*," *J. Biomed. Opt.* **12**, 044006-1–044006-7 (2007).
30. D. B. Murphy, *Fundamentals of Light Microscopy and Electronic Imaging*, Wiley-Liss, New York (2001).
31. C. Preza, "Rotational-diversity phase estimation from differential-interference-contrast microscopy images," *J. Opt. Soc. Am. A* **17**(3), 415–424 (2000).
32. M. R. Arnison, C. J. Cogswell, N. I. Smith, P. W. Fekete, and K. G. Larkin, "Using the Hilbert transform for 3D visualization of differential interference contrast microscope images," *J. Microsc.* **199**, 79–84 (2000).
33. M. R. Arnison, K. G. Larkin, C. J. Sheppard, N. I. Smith, and C. J. Cogswell, "Linear phase imaging using differential interference contrast microscopy," *J. Microsc.* **214**, 7–12 (2004).
34. B. Heise, A. Sonnleitner, and E. P. Klement, "DIC image reconstruction on large cell scans," *Microsc. Res. Tech.* **66**, 312–320 (2005).
35. H. Ishiwata, M. Itoh, and T. Yatagai, "A new method of three-dimensional measurement by differential interference contrast microscope," *Opt. Commun.* **260**, 117–126 (2006).
36. M. Shribak and S. Inoue, "Orientation-independent differential interference contrast microscopy," *Appl. Opt.* **45**(3), 460–469 (2006).
37. P. Quinn and F. C. Horstman, "Is the mouse a good model for the human with respect to the development of the preimplantation embryo *in vitro*?" *Hum. Reprod.* **13**(Suppl. 4), 173–183 (1998).
38. K. M. Ebert, R. E. Hammer, and V. E. Papaioannou, "A simple method for counting nuclei in the preimplantation mouse embryo," *Experientia* **41**(9), 1207–1209 (1985).

39. D. O. Hogenboom, C. A. DiMarzio, T. J. Gaudette, A. J. Devaney, and S. C. Lindberg, "Three-dimensional images generated by quadrature interferometry," *Opt. Lett.* **23**(10), 783–785 (1998).

40. C. DiMarzio, "Optical quadrature interferometry utilizing polarization to obtain in-phase and quadrature information," U.S. Patent No. 5,883,717 (Mar. 16, 1999).

41. C. DiMarzio, "Optical quadrature interferometer," U.S. Patent No. 6,020,963 (Feb. 1, 2000).

42. J. A. Newmark, W. C. Warger II, C. Chang, G. E. Herrera, D. H. Brooks, C. A. DiMarzio, and C. M. Warner, "Determination of the number of cells in preimplantation embryos by using noninvasive optical quadrature microscopy in conjunction with differential interference contrast microscopy," *Microsc. Microanal. Microstruct.* **13**(2), 118–127 (2007).

43. D. Ghiglia and M. Pritt, *Two-Dimensional Phase Unwrapping: Theory, Algorithms, and Software*, Wiley, New York (1998).

44. A. A. Lebedeff, "Polarization interferometer and its applications," *Rev. Opt., Theor. Instrum.* **9**, 385 (1930).

45. E. Cuche, F. Bevilacqua, and C. Depeursinge, "Digital holography for quantitative phase-contrast imaging," *Opt. Lett.* **24**(5), 291–293 (1999).

46. C. J. Mann, L. Yu, and M. K. Kim, "Movies of cellular and subcellular motion by digital holographic microscopy," *Biomed. Eng. Online* **5**, 1–10 (2006).

47. F. Charrière, A. Marian, F. Montfort, J. Kuehn, T. Colomb, E. Cuche, P. Marquet, and C. Depeursinge, "Cell refractive index tomography by digital holographic microscopy," *Opt. Lett.* **31**(2), 178–180 (2006).

48. G. Popescu, L. P. Deflores, J. C. Vaughan, K. Badizadegan, H. Iwai, R. R. Dasari, and M. S. Feld, "Fourier phase microscopy for investigation of biological structures and dynamics," *Opt. Lett.* **29**(21), 2503–2505 (2004).

49. T. Ikeda, G. Popescu, R. R. Dasari, and M. S. Feld, "Hilbert phase microscopy for investigating fast dynamics in transparent systems," *Opt. Lett.* **30**(10), 1165–1167 (2005).

50. I. Yamaguchi and T. Zhang, "Phase-shifting digital holography," *Opt. Lett.* **22**(16), 1268–1270 (1997).

51. A. Dubois, L. Vabre, and A. C. Boccara, "Sinusoidally phase-modulated interference microscope for high-speed high-resolution topographic imagery," *Opt. Lett.* **26**(23), 1873–1875 (2001).

52. D. Paganin and K. A. Nugent, "Noninterferometric Phase imaging with partially coherent light," *Phys. Rev. Lett.* **80**(12), 2586–2589 (1998).

53. A. Barty, K. A. Nugent, D. Paganin, and A. Roberts, "Quantitative optical phase microscopy," *Opt. Lett.* **23**(11), 817–819 (1998).

54. C. L. Curl, C. J. Bellair, T. Harris, B. E. Allman, P. J. Harris, A. G. Stewart, A. Roberts, K. A. Nugent, and L. M. D. Delbridge, "Refractive index measurement in viable cells using quantitative phase-amplitude microscopy and confocal microscopy," *Cytometry* **65A**, 88–92 (2005).

55. D. S. Marx and D. Psaltis, "Polarization quadrature measurement of subwavelength diffracting structures," *Appl. Opt.* **36**(25), 6434–6440 (1997).

56. Z. Yaqoob, J. Wu, X. Cui, X. Heng, and C. Yang, "Harmonically-related diffraction gratings-based interferometer for quadrature phase measurements," *Opt. Express* **14**(18), 8127–8137 (2006).

57. N. Nagy, M. Gertsenstein, K. Vintersten, and R. Behringer, *Manipulating the Mouse Embryo*, Cold Spring Harbor Laboratory Press, Cold Spring Harbor, NY (2003).

58. K. A. Rafferty, Jr., *Methods in Experimental Embryology of the Mouse*, p. 82, John Hopkins University Press, Baltimore, MD (1970).

59. J. Tao, R. Tamis, K. Fink, B. Williams, T. Nelson-White, and R. Craig, "The neglected morula/compact stage embryo transfer," *Hum. Reprod.* **17**(6), 1513–1518 (2002).